Materials Science-Poland, 42(2), 2024, pp. 26-40
http://www.materialsscience.pwr.wroc.pl/
DOI: 10.2478/msp-2024-0017

Effect of solution and artificial aging heat treatment on the hardness, friction and wear properties of laser cladding and roll-formed 18Ni300 materials

Zhaoqing Tang, Weimin Li, Zeyu Yang*, Jinying Wang

School of Mechanical Engineering and Automation, Liaoning University of Technology, Jinzhou Liaoning 121001, China

18Ni300 is widely used in precision moulds, national defence, and other engineering fields due to its high strength and toughness, and because its properties can be greatly changed after heat treatment. In this research, the 18Ni300 cladding layer was fabricated on 18Ni300 substrate using the laser cladding method and a solid solution artificial aging treatment was carried out to analyse its macro morphology and metallographic organization. Comparison of hardness, friction, and wear of cladding layers manufactured by laser cladding and of materials produced by rolling was performed before and after heat treatment. The results show that the solution and artificial aging heat treatment has a significant effect on the microstructure of the cladding layer fabricated by laser cladding. There are obvious differences in the organization and morphology of different parts of the cladding layer before heat treatment; the metallographic organization and morphology of different parts of the cladding layer after heat treatment are the same. The trend of change of material hardness before and after heat treatment is the same in that the cladding layer is greater than the rolled material and the hardness of the material after heat treatment is much greater than the hardness of the material before heat treatment. The hardness and wear resistance of the material after solution and artificial aging heat treatment has been significantly improved, and the impact on the rolled production material of the melted cladding layer manufactured by laser cladding is even greater.

Keywords: *maraging steel, laser cladding, solution and artificial aging heat treatment, frictional wear*

1. Introduction

Additive manufacturing is an important development trend of modern industry and an indispensable part of intelligent manufacturing [1]. Laser cladding is the most common additive manufacturing technology, and one that has been widely used in many fields for its advantages of good moulding performance and high degree of design freedom it provides [2]. It is not only used to repair surface defects in equipment such as aircraft engines and to manufacture high-strength and corrosion-resistant aerospace parts to enhance safety and reliability, but also used in the automotive industry to enhance the durability of parts by preparing coatings for engines and transmissions. Martensitic aging steel, known for its high strength, high toughness, and retention of ductility, is a major consumer material in high-end technology fields such as aerospace, the nuclear industry, and high-end mould making. Recent years, with its consumption rising year by year, have fully demonstrated the huge market potential and broad application prospects of martensitic aging steel [3]. 18Ni300 is a martensitic aging steel manufactured after solid solution aging heat treatment. It has the advantages of good toughness, small thermal deformation, and high strength [4]. Because of its material properties, martensitic aging steel is particularly suitable for the laser additive manufacturing process used in the production of parts with excellent strength, hardness, and thermal stability needs, so domestic and foreign scholars are actively involved in additive manufacturing research and development of martensitic aging steel. In the future, how to further reduce the cost and energy consumption and shorten the design cycle to realize the high-performance manufacturing of maraging aging steel on the basis of ensuring the material

* E-mail: 1552613466@qq.com

© Zhaoqing Tang et al. 2024. This is an open access article distributed under the Creative Commons Attribution-NonCommercial-NoDerivatives 4.0 License. (http://creativecommons.org/licenses/by-nc-nd/4.0/)

properties has become the main research content and development direction in this field [5]. During the laser cladding process, however, the cladding layer fabricated by laser cladding is prone to defects such as cracks [6, 7] and porosity [8, 9], which are detrimental to the material properties as a result of the complex variations in the moulding experience. Numerous scholars have conducted experiments on 18Ni300 materials using various process parameters for laser cladding [10], optimizing their process parameters while employing diverse testing methods. They have conducted extensive testing and analysis on the metallographic structure of the 18Ni300 cladding layer [11], including mechanical properties [12], defect analysis [13], and corrosion resistance [14], ultimately achieving improved properties [15].

In research related to 18Ni300 laser cladding, most scholars have focused directly on the study of the cladding layer produced through laser cladding manufacturing, with little attention paid to the heat treatment of laser cladding materials. However, heat treatment of martensitic aging steel is crucial for enhancing the performance of this material. Therefore, this research aims to explore the impact of heat treatment on the metallurgical structure of the cladding layer through the manufacturing of a multichannel 18Ni300 cladding layer using laser cladding, followed by solid solution aging heat treatment. Additionally, hardness measurements and friction and wear experiments were conducted on the laser cladding-manufactured 18Ni300 cladding layer before and after heat treatment, to reveal the effect of heat treatment on its performance. This study aims to provide reference and guidance for additive manufacturing research of martensitic aged steel. The wear volume of the material is calculated from the contour of the wear marks obtained by a 3D profiler. The wear rate is calculated with the following formula:

$$W = \frac{V}{FL}$$

In the formula, W is the wear rate of the material, V the wear volume of the material, F the applied load, and L the sliding distance.

Table 1. Elemental composition of 18Ni300 powder (wt%)

Ni	Co	Mo	Ti	Al	Cr	P	Mn	Si	C	S	Fe
18.3	8.9	4.7	0.70	0.20	0.10	0.05	0.02	0.03	0.05	0.03	Bal.

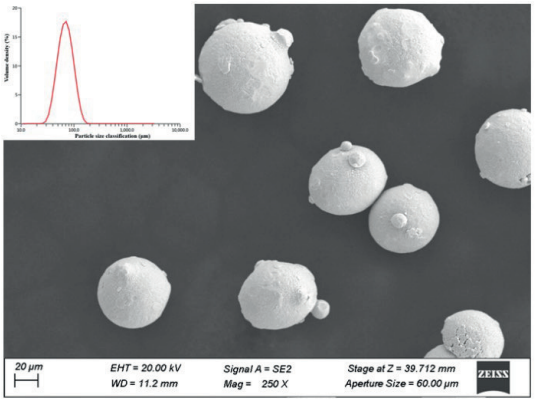


Fig. 1. Microscopic morphology of 18Ni300 powder

2. Experimental design

2.1. Experimental materials

The experiment employed 18Ni300 powder produced by VILORY Co. Its elemental composition is presented in Table 1, while the powder morphology is depicted in Figure 1. The powder had a particle size ranging from 45 to 105 micrometers. The powder was laser-cladded onto an 18Ni300 substrate that had been rolled by Bao steel Iron and Steel Company Limited. Prior to the experiment, the surface of the substrate was polished to eliminate the potential influence of surface impurities and oxidized layers on the experiment. In addition, the powder was placed in a vacuum drying oven for drying before the experiment.

2.2. Experimental method

The experimental instruments used were the YLR-3000 laser, KUKA robot, FHPF-10 synchronized powder feeder, etc. Nitrogen was used as a protective gas. In the experimental process, the powder is driven by the powder feeding gas through the synchronized powder feeder and is ejected from the powder injection port of the laser cladding head to the substrate while interacting with the high-energy laser beam to form a molten pool, which is

Table 2. Experimental process parameters

Laser power W	Scan speed mm/s	Speed of power feeding g/min	Sweep spacing mm
1300	2	10	0.6

moved by the KUKA robot in accordance with the preprogrammed paths to finally form the desired cladding material. The experimental parameters of this laser cladding experiment were based on previous research [16, 17], and are shown in Table 2, and the experimental design path scheme is shown in Figure 2(a).

The 18Ni300 cladding layer manufactured by laser cladding and the 18Ni300 material produced by rolling were cut into shapes convenient for subsequent experiments using wire-cutting technology. These were then heat-treated through solid solution aging in a muffle furnace. Taking into account the material properties, the heat treatment parameters were selected based on Xiang [18]: solid solution at 820°C for 1 hour, followed by aging at 480°C for 4 hours, as shown in Figure 2(b). The heat-treated cladding layer samples were cut into shapes suitable for polishing using wire-cutting technology. The cross-section of the cladding layer manufactured by laser cladding was polished several times with 600–2000 grit mesh sandpaper both before and after heat treatment, and then further polished using a metallographic grinding and polishing machine until the surface was free of obvious scratches. Aqua regia was used to etch the polished surface, and finally the surface was cleaned with industrial alcohol and dried. The 18Ni300 material produced by rolling (RM), the 18Ni300 cladding layer manufactured by laser cladding (LCM), the 18Ni300 material produced by rolling after heat treatment (HRM), and the 18Ni300 cladding layer manufactured by laser cladding after heat treatment (HLCM) were subjected to friction and wear experiments in an Rtec-5000 friction and wear experimental machine using the rotary dry friction method. This experimental method involves fixing the material under testing at the center of the disc and simulating dry friction conditions by placing grinding balls and applying loads while the disc is rotating, while recording the relevant data during the experiment in real time. Prior to the friction wear test, the specimens were polished on a grinding machine to remove the surface oxidation layer and ensure surface flatness, minimizing errors caused by other factors. A Ø6 mm GCr15 grinding ball was utilized in the friction and wear experiments, applying a load of 10 N and rotating with a radius of 5 mm at 120 rpm for 1 hour. The friction coefficient was recorded throughout the experiments, and the volumetric wear rate was measured upon completion of the experiments.

3. Discussion of experimental results

3.1. Macroscopic morphology, metallographic organization, and XRD analysis of the cladding layer

Figure 3 shows the macro morphology of the cladding layer manufactured by laser cladding. In the figure, it can be seen that the experimental effect is better, and there is no obvious depression or elevation between the adjacent fusion channels of the cladding layer, which forms a highly flat plane with no obvious defects. The lap effect is also good. A suitable lap effect can improve the surface quality of the cladding layer [19], which facilitates the subsequent experiments. Given that the melting point of the 18Ni300 cladding layer, as reported by Luo et al. [20], exceeds the temperature attained during heat treatment, the macroscopic shape of the cladding layer remains unchanged following the heat treatment process.

Figure 4(a) shows the cross-sectional morphology of the cladding layer, from which it can be seen that the bottom of the cladding layer bonds with the substrate without fusion defects. Therefore, the bonding effect is better, which prevents stress concentration and cracks from sprouting [21, 22]. Figure 4(a1) and (a4) correspond to the position of the top of the cladding layer; Figure 4(a2) and (a5) correspond to the position of the central part; and Figure 4(a3) and (a6) correspond to the bottom. Figure 4(a1) to (a3) represent the metallographic structure of the cladding layer before heat

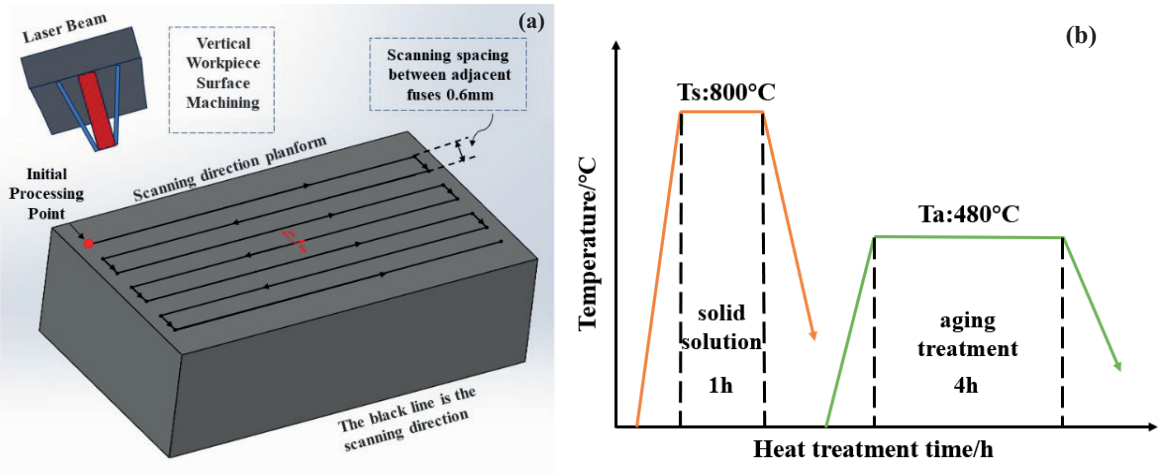


Fig. 2. (a) schematic diagram of the experimental design path scheme; (b) heat treatment scheme

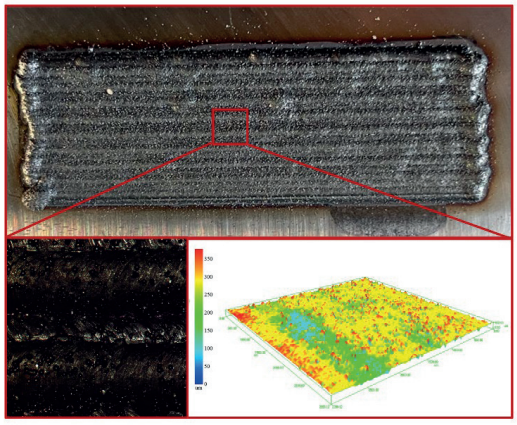


Fig. 3. Macroscopic morphology of the cladding layer

treatment, and Figure 4(a4) to (a6) represent the metallographic structure of the cladding layer after heat treatment. Because of the uneven temperature distribution and heat dissipation during the laser cladding process, there are obvious differences in the microstructure of the cladding layer at different locations [23]. The dendritic microstructure observed in Figure 4(a1) is attributed to the direct contact between the top of the cladding layer and the surrounding environment during the process, resulting in better heat dissipation and a faster cooling rate. According to the solidification theory, this rapid cooling process effectively hinders grain growth and leads to grain organization aggregation and refinement. The microstructure in Figure 4(a2) consists of both dendritic and columnar crystals. The high cooling rate of the molten pool leads to dynamic nonequilibrium crystallization, with some fine dendritic cells crystallizing before they can grow large enough to develop into fine dendritic structures. The relatively coarse columnar dendrites grow in the direction of the laser scanning trajectory, but often due to the uneven temperature distribution and reheating by the laser heat source, they may exhibit changes in growth direction [24]. In addition, due to the differences in residual temperatures and lap heights at different locations of the cladding layer during the lap forming process, this leads to variations in the heating conditions and the direction of heat flow, which also affects the direction of grain growth [25]. The metallographic organization in Figure 4(a3) shows columnar dendrites perpendicular to the fusion line with a small number of cytosolic crystals. During the laser cladding process, there is a large temperature gradient in the vertical direction of the cladding layer due to the thermal conductivity of the substrate, and the solidification rate is low. This large temperature gradient to solidification rate ratio promotes rapid tissue growth in this direction. The presence of a clearly visible fusion line at the junction of the cladding layer and the substrate demonstrates that excellent metallurgical bonding between the cladding layer and the substrate was achieved [26]. Figure 4(a4) to (a6) shows that

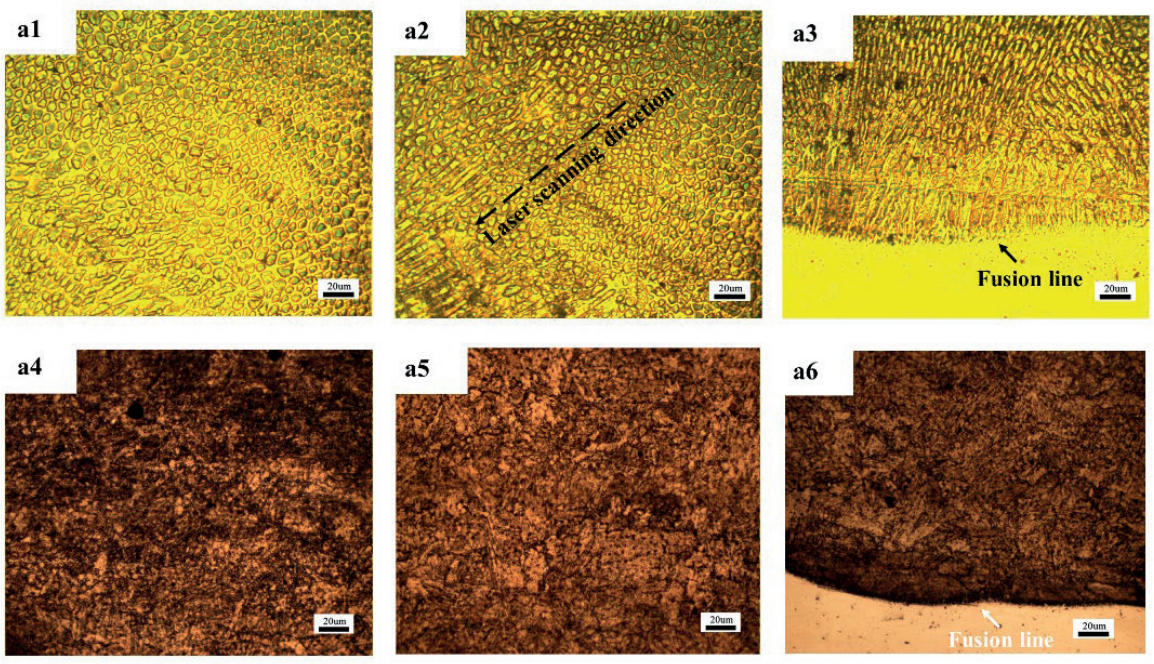


Fig. 4. Microstructure of cladding layer before and after heat treatment

the metallographic organization of the cladding layer after solid solution aging heat treatment has changed greatly relative to that before heat treatment, and the fusion line at the junction of the cladding layer and the substrate is still obvious, which shows the second-phase strengthening [27]. At this time, the metallographic organization of the various parts of the cladding layer has the same morphology, and the fine precipitates formed during the heat treatment are distributed between the grain boundaries and laths, forming dense lath martensite accompanied by a small amount of residual austenite organization. After solid solution aging heat treatment, the grain boundary structure of the cladding layer becomes relatively unclear, and the shape is also relatively irregular. The main reason is that the resulting precipitation phase, after the heat treatment, squeezes the grain boundaries, releases residual stresses, and causes phase transformation [28]. Although the martensite laths have a tendency to decompose, the overall lath morphology is maintained. During heat treatment, the martensitic transformation is inhibited due to the microscopic segregation of the Ni element, leading to the presence of a small portion of residual austenite [29]. The disappearance of the dendritic morphology and the interface characteristics of the laser scanning trajectory after solid solution aging heat treatment are attributed to the precipitation of the second phase during the heat treatment process. This precipitation destabilizes the internal structure and produces a squeezing effect on the grain boundaries, destroying the characteristics of the grains [30].

Figure 5 shows the XRD diffraction patterns of the cladding layer, both before and after heat treatment, scanned between 30° and 90°. As is evident from the figure, crystallization peaks of the cladding layer appear at diffraction angles of approximately 44°, 51°, and 75° both pre- and post-treatment. Comparing the diffraction angles and intensities of these peaks identifies the material phase as Co, with crystallographic indices (111), (200), and (220). Additionally, peaks at angles around 45°, 65°, and 83° correspond to the phases of Fe and Fe_7Ni_3, with indices (110), (200), and (211). On the basis of the material's Fe and Ni compositional ratios, these peaks are interpreted as overlapping peaks of α-Fe and Fe_7Ni_3. The cladding layer, as shown in Figure 5, comprises

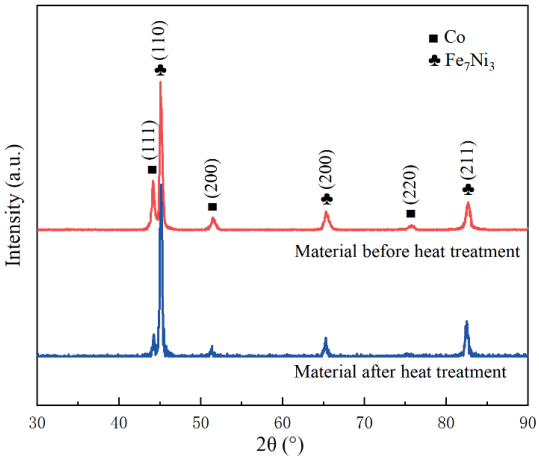


Fig. 5. XRD diffraction pattern of the cladding layer before and after heat treatment

Co, α-Fe, and Fe_7Ni_3. Heat treatment modifies the austenite content in the layer, promoting a phase transition from austenite to martensite [31]. Notably, the diffraction peaks of α-Fe at 200 and 211 exhibit increased intensity, indicating the occurrence of the austenite-to-martensite transition, as γ-Fe is not detected [32]. Furthermore, compared to the untreated cladding layer, the diffraction intensity of Co's characteristic peaks decreases after heat treatment, suggestive of a lower relative Co content and a higher relative content of α-Fe and Fe_7Ni_3, favouring the thorough mixing of Fe and Ni elements.

3.2. Analysis of cladding layer hardness and wear resistance

Figure 6(a) shows the hardness curves of the material before and after heat treatment, where the hardness values of each region are measured from the top down of the cross-section of the cladding layer. The load applied to each measurement is 100 g, the duration is 12 s, and the measurement interval is 0.15 mm. It can be observed in Figure 6(a) that both curves exhibit a similar trend, with the hardness of the laser cladding layer exceeding that of the rolled material. This is attributed to the finer grains in the laser cladding layer, which, compared to the rolled material, results in a larger grain boundary area that strengthens the intermetallic bonding force, significantly hindering dislocation movement and thereby enhancing the material's hardness [33]. The microhardness of the fusion area between the cladding and the substrate starts to decrease, due to the fact that under the continuous action of the laser beam, the cladding, and the substrate are bonded to each other, the elements diffuse into each other, and the degree of bonding farther away from the substrate is lower, thus leading to a decrease in the hardness. The hardness of the cladding layer and substrate after heat treatment was significantly improved, which is in line with the results of the study conducted by Li et al. [34]. As depicted in Figure 6(b), it can be observed that the hardness of the cladding layer following solid solution aging heat treatment is the highest, with an average hardness of 476.8 Hv. This represents a 50.2% increase compared to the average hardness of the 18Ni300 material manufactured by laser cladding before heat treatment. The average hardness of the material produced by rolling after heat treatment is 370 Hv, which is 24.1% higher than the average hardness of the material produced by rolling before heat treatment. It has been proved that heat treatment has more influence on the hardness of laser cladding than on that of rolling material.

Figure 7 shows the friction coefficients of the 18Ni300 cladding layer fabricated by laser cladding before and after heat treatment and the 18Ni300 material produced by rolling. As can be seen from Figure 7(a), when the friction and wear experiments were just started, the trend of friction coefficients of all four materials increased sharply. At this stage, theoretically the grinding ball and the specimen should be face to face, but in practice, because the surface contact between the friction vice and the specimen is not close enough, both of them provide only sliding friction with point contact, resulting in a small contact area and high stress, under which the specimen and the grinding ball are constantly colliding under the pressure. This produces a large amount of abrasive debris, making the friction coefficient show a rising trend, and the surface is experiencing the abrasive wear stage. With the passage of time, the surface gradually becomes smoother, the friction vice fit effect

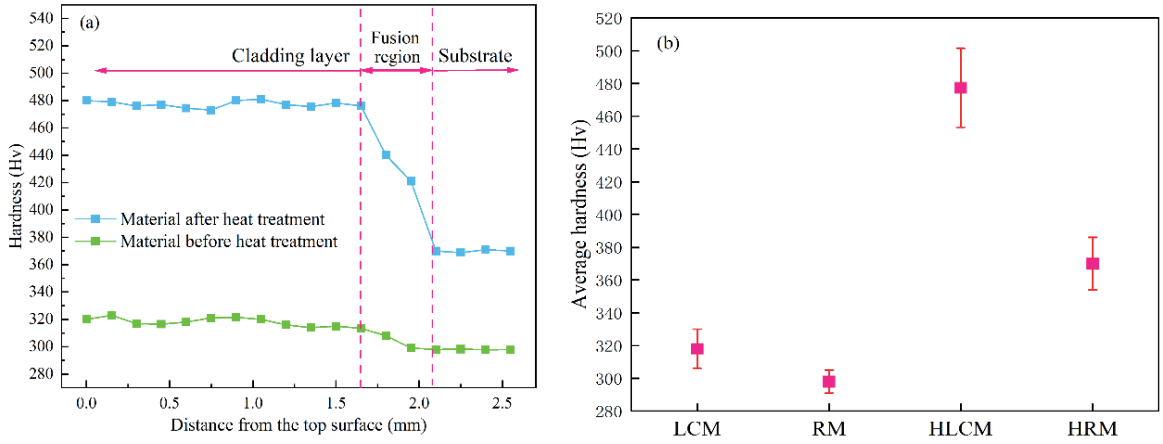


Fig. 6. Hardness plots of an 18Ni300 cladding layer fabricated by laser cladding before and after heat treatment and 18Ni300 material produced by rolling: (a) hardness curve; (b) average microhardness

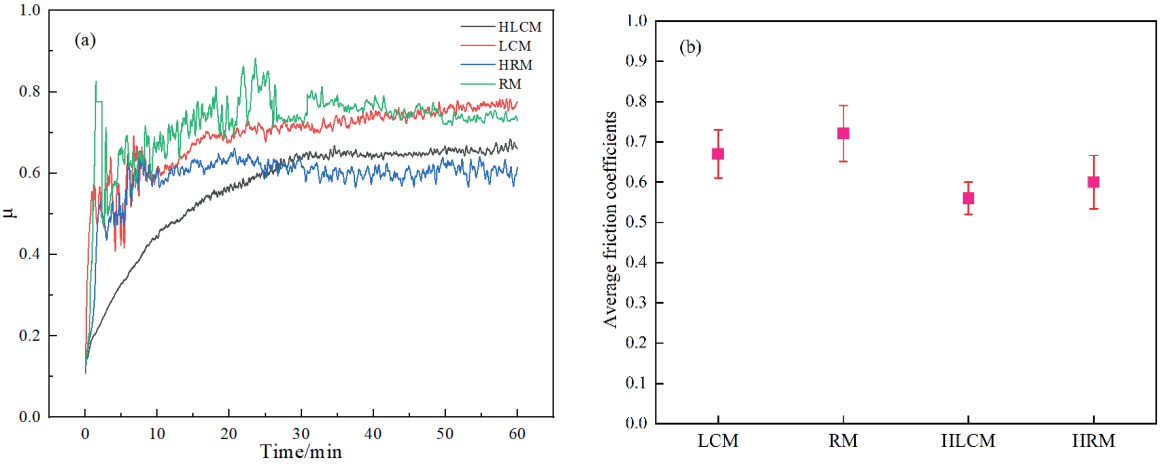


Fig. 7. Friction coefficients of 18Ni300 cladding layer manufactured by laser cladding and 18Ni300 material produced by rolling before and after heat treatment: (a) coefficient of friction; (b) average coefficient of friction

is improved, the friction coefficient fluctuation is small, and the wear conditions are relatively stable. This time creates the actual friction coefficient [35], and the surface is experiencing the stable wear stage. In the four types of coating before heat treatment rolling production of 18Ni300 material friction coefficient fluctuation is the largest, because the size of the coefficient of friction is related to the quality of the material [36]. In the process of rolling production of easy to stress concentration caused by cracks, inclusions, bubbles, and other defects within the material, the quality of the material is poor. Moreover, the hardness of this material is relatively low, the surface of the material is rapidly damaged, and the surface of the substrate becomes rough and susceptible to abrasion, reflecting a high coefficient of friction, which has a large impact on the fluctuation of the friction factor. Combined with Figure 7(b), analysis shows that the average friction coefficient of 18Ni300 material produced by rolling before heat treatment is the highest 0.721, and the average friction coefficient of the material after heat treatment is smaller than the average friction coefficient before heat treatment. The fluctuation of the friction coefficient of the 18Ni300 cladding layer manufactured by laser

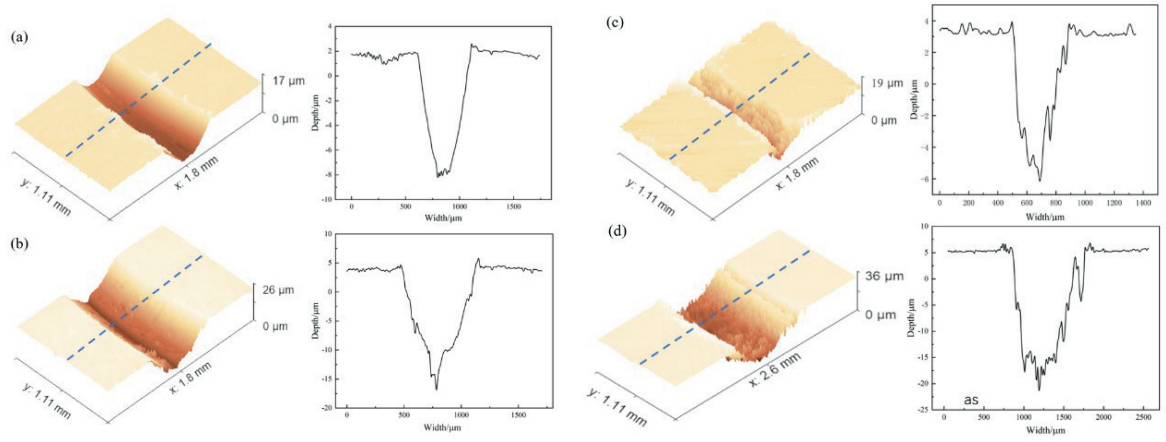


Fig. 8. Wear 3D profile morphology and wear profile of the material: (a)18Ni300 cladding layer produced by laser cladding after heat treatment; (b)18Ni300 cladding layer produced by laser cladding; (c)18Ni300 material produced by rolling after heat treatment; (d)18Ni300 material produced by rolling

cladding after heat treatment was the smallest, and the average friction coefficient was the smallest at 0.562.

Figure 8 shows that the wear pattern for the heat treatment before and heat treatment after laser cladding of the manufactured 18Ni300 cladding layer and the wear pattern of the rolling production of 18Ni300 material differ in their three-dimensional profile morphology and wear profile. Different materials, after the same friction and wear experiments, demonstrate significant changes in their wear morphology. Figure 8(a) and 8(c) show a wear profile width of a narrower "V" type; Figure 8(b) and 8(d) show a wear profile width of a larger "U" type. This is because after heat treatment, the material will form a finer and denser martensitic organization, which greatly increases its hardness and improves the wear resistance of the material, and thus the wear marks are narrower. The cladding layer Figure 8(a) produced by laser cladding after heat treatment has the shallowest wear marks and relatively smooth edges, showing good wear resistance. The cladding layer Figure 8(b) produced by laser cladding before heat treatment showed significantly heavier wear marks and narrower grooves at the bottom of the wear marks than Figure 8(a). This is because when a constant stress is applied to the specimen, scratches and abrasive chips are initially formed on the surface of the specimen, and the friction debris generated between the specimen and the grinding ball will gradually form grooves under the action of compressive stress. Over time, the abrasive debris is subjected to a continuous downward pressure resulting in the reduction of the contact area of the grinding ball, and the surface of the specimen produces narrower grooves. Comparison with the material Figure 8(c) produced by rolling after heat treatment, the material Figure 8(d) produced by rolling before heat treatment showed wide and deep furrows on the surface of the abrasion marks, and the surface after frictional abrasion produced obvious flaking. It is because the hardness of the material produced by rolling before heat treatment is lower, and the contact stress between the material and the grinding ball is larger under prolonged interaction, which is more likely to produce the accumulation of abrasive debris. The exfoliated abrasive debris strengthened the force on the surface during the frictional wear process, which made the surface wear more severe [37], producing a scaly and laminated surface.

Figure 9 shows the wear rate of 18Ni300 cladding layers manufactured by laser cladding and 18Ni300 material produced by rolling before heat treatment and after heat treatment. This wear rate is an average calculated based on a series of experimental data. In the figure, the magnitude of wear rate in the 18Ni300 cladding layer manufactured by laser cladding after heat treatment is greater than

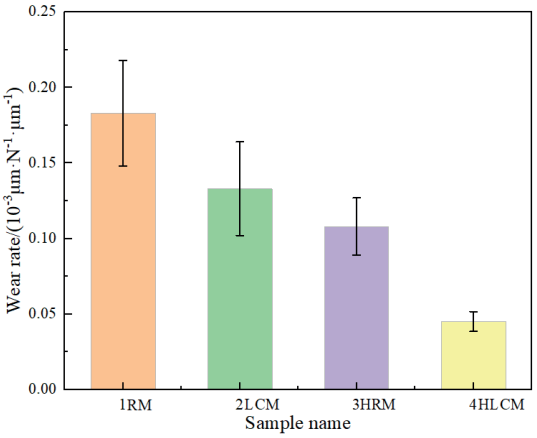


Fig. 9. Wear rate of 18Ni300 cladding layer fabricated by laser cladding and 18Ni300 material produced by rolling before and after heat treatment

that of the 18Ni300 material produced by rolling after heat treatment. The wear resistance of the 18Ni300 cladding layer made by laser cladding after heat treatment is better than that of other materials; its wear rate is only 0.045. On the one hand, this is because the hardness of this material is much higher than that of other coatings, and on the other hand, it is because during the heat treatment process, the material forms a large number of high-density dislocations contained in the material and a finer grain lath martensite, which gives it better resistance to abrasion. The wear rate of 18Ni300 material produced by rolling is a maximum 0.183, which is poor wear resistance. According to Archard's wear theory, when the friction distance and the applied load are certain, the wear rate of the material is inversely proportional to the hardness of the material [38], so the lower the hardness of the material, the worse its wear resistance. Comparison with Figure 7 found that the friction factor fluctuation amplitude of 18Ni300 material produced by rolling is the largest, and due to the uneven force on the surface of the workpiece, a large number of deep, irregular pits appear on the surface of the workpiece after wear, and therefore the surface damage is serious, which is the reason for the large fluctuation of its friction factor. The wear rate of the 18Ni300 cladding layer made by laser cladding after heat treatment was reduced by 66.1% compared to that before heat treatment, and the wear rate of the material produced by rolling after heat treatment was reduced by 41.2% compared to that before heat treatment. Therefore, the heat treatment had a greater impact on the wear rate of the cladding layer made by laser cladding than that of the material produced by rolling.

Figure 10 shows the abrasion morphology and energy-dispersive X-ray (EDS) results after the friction and wear experiments, from which it can be seen that each material has the highest content of Fe elements, and that the surface shows different degrees of oxide film. The surface of Figure 10(a) shows deeper furrows with lamellar spalling, and the surface damage is particularly severe with wider abrasion marks compared to the other materials. On the one hand, this is because the hardness of this material is lower than that of other materials, and on the other hand, the material is prone to internal defects during the rolling process, which together result in a material that is susceptible to wear. Inhomogeneous oxidative wear during friction makes the material less wear-resistant [39] by making the surface material more susceptible to spalling and damage, leading to its elevated wear rate. EDS results show that the Gr elemental content of the wear surface of this material is higher than the Gr elemental content of the other surfaces. Combined with the friction coefficient of Figure 7 analysis, rolling production of material friction and wear coefficient is larger, fluctuation is obvious, the specimen and grinding ball subjected to the force is large and irregular, the surface damage is serious, the surface of the material and the grinding ball are subjected to violent contact, and the grinding ball sticks in the surface of the material during processing, increasing the surface of the Gr elements, adhesive wear occurred. From Figure 10(b), it can be seen that the width of the abrasion marks on the surface of the material is obviously narrowed, and all the local areas show the typical fatigue wear characteristics of fish scale. Some short and shallow furrows and spalling can also be observed on the surface, which proves that fatigue wear and abrasive wear occurred on the surface [40]. From Figure 10(c), it can be seen that there are a large number of deep and long furrows distributed on the surface of the material, and the width of the surface

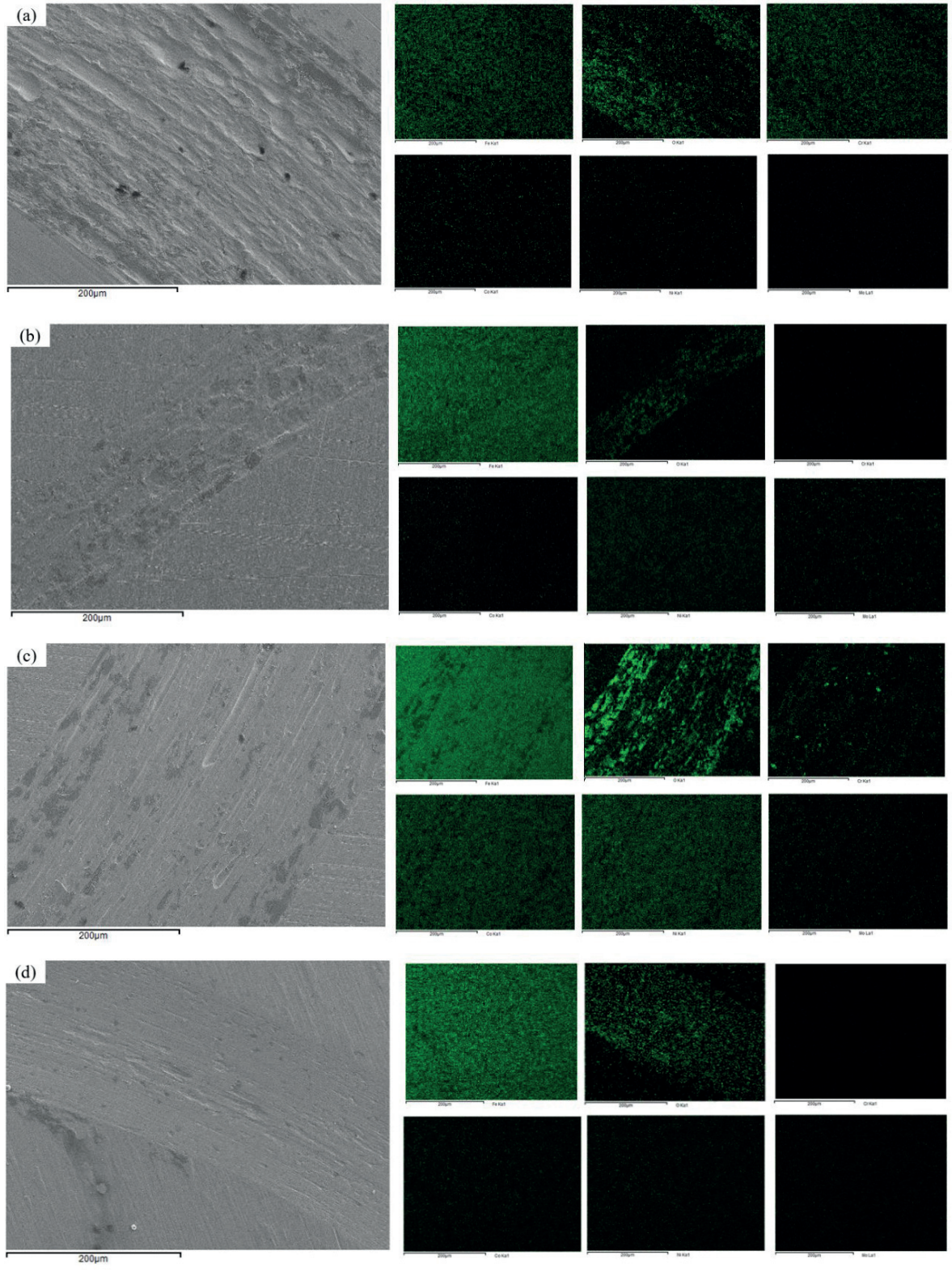


Fig. 10. Abrasion morphology and EDS results after friction and wear experiments: (a)18Ni300 material produced by rolling; (b)18Ni300 material produced by rolling after heat treatment; (c)18Ni300 cladding layer produced by laser cladding; (d)18Ni300 cladding layer produced by laser cladding after heat treatment

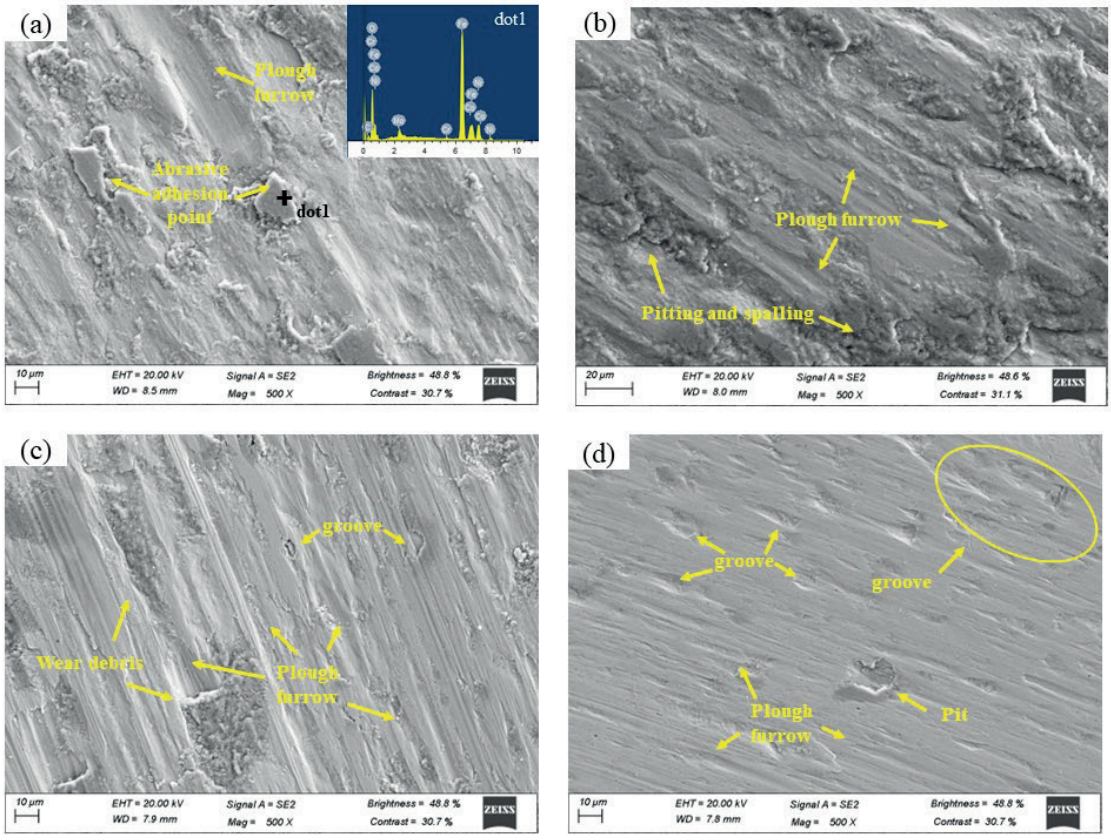


Fig. 11. SEM morphology of the abraded surface after the friction experiment: (a) 18Ni300 material produced by rolling; (b) 18Ni300 material produced by rolling after heat treatment; (c) 18Ni300 cladding layer produced by laser cladding; (d) 18Ni300 cladding layer produced by laser cladding after heat treatment.

wear is wide; the EDS results show a nonuniform distribution of surface oxygen elements, and this distribution is the same as the oxygen distribution pattern in Figure 10(a). Gr elements show point-like aggregation, which proves that adhesive wear occurs on the surface. Figure 10(d), shows that the material surface is the smoothest and most flat in comparison with the other materials, with only shallow grooves and slight abrasive wear occurring on the surface. The EDS results showed that the distribution of oxygen elements on its wear surface did not show nonuniform oxidation as shown in Figure 10(a) and Figure 10(c), but exhibited a uniform distribution of oxygen elements. As the friction time increases, the deformation and warming of the material surface promotes the generation of an oxide film between the friction partner and the ambient medium, which improves the abrasion resistance and thus reduces the wear rate of the material.

Figure 11 shows the SEM morphology of the abraded surface after the friction experiment, from which it can be seen that the removal of the wear surface of the material before and after the heat treatment has changed significantly from the principle. A wide and deep furrow appears on the surface in Figure 11(a), and the EDS dot scans showed that the surface adhered to large pieces of Gr elements. Because of the low hardness of this material weak resistance to adhesion, in the friction process occurred plastic deformation matrix and abrasive chips occurred cold welding [41]. When the bonding force of the adhesion point is less than the interacting shear force, it makes the adhesion point on the wear surface of the substrate sliding, and in the sliding, it pushes the substrate to produce

plastic flow, forming a wide and deep furrow, and the surface damage is serious. In contrast to Figure 11(a), Figure 11(b) produces significantly less sticky conditions, and the furrows are relatively shallow and narrow, with the surface material spalling off due to fatigue. After a long period of wear, the surface produces pitting and spalling under interaction, reflecting obvious fatigue wear characteristics. The surface in Figure 11(c) shows obvious edge irregularity furrows with adhesion, which is a removal of ductility and continuity, and abrasive debris sticking to the material surface. The best surface flatness is seen in Figure 11(d) of the heat treated material, which shows brittle removal with short plough furrows, and pits created by abrasive chips in contact with the surface. Since hardness and abrasion resistance are directly correlated, the higher hardness of Figure 11(d) can be determined by observing the morphology of the removal.

4. Conclusions

By means of solid solution aging heat treatment of the cladding layer made by laser cladding and the material produced by rolling, the changes in the metallographic organization of the cladding layer before and after the heat treatment were investigated, and the hardness test and friction and wear experiments were carried out on the material to study the effect of heat treatment. The principal conclusions are as follows:

1. The solid solution aging heat treatment has a significant effect on the metallographic organization of a cladding layer that has been manufactured by laser cladding. The cladding layer before heat treatment consists of cellular crystals, equiaxed crystals, and dendritic crystals, and there are obvious differences in the organization and morphology of different positions. After heat treatment, the cladding layer consists of dense lath martensite and a small amount of residual austenite, and the organization and morphology of different positions are the same. The cladding layer contains Co, α-Fe, and Fe_7Ni_3 intermetallic compounds.
2. The hardness of the cladding layer and the substrate after solid solution aging heat treatment was significantly improved; the hardness of the cladding layer when manufactured by laser cladding was greater than the hardness of the material produced by rolling. The maximum hardness of the heat-treated cladding layer is 477.2 Hv, which is 50.2% higher than the hardness of the cladding layer before heat treatment. The hardness of the rolled material after heat treatment is 370 Hv, compared with the average increase in hardness of 24.1% before heat treatment, proving that the heat treatment of the cladding layer in laser cladding manufacture has a greater impact on the hardness of the material than on the rolled production cladding layer.
3. Before and after the solution-aging heat treatment, the wear pattern of the material changed significantly, with the wear profile of the material after heat treatment being narrower and "V"-shaped, and the wear profile of the material after heat treatment being larger and "U"-shaped. After heat treatment, the cladding layer has the shallowest wear marks and relatively smooth edges, with a minimum wear rate of only 0.045, showing good wear resistance. The surface of the abrasion mark of the material produced by rolling before heat treatment showed wide and deep furrows, and the surface after friction abrasion produced obvious flaking, with a maximum wear rate of 0.183. The wear rate of the 18Ni300 cladding layer made by laser cladding after heat treatment was reduced by 66.1% compared with that before heat treatment, and the wear rate of the material produced by rolling before heat treatment was reduced by 41.2% compared with that before heat treatment. This proves that the heat treatment has a greater effect on the wear rate of the cladding layer manufactured by laser cladding than that of the material produced by rolling.

4. Before heat treatment, the wear surface of 18Ni300 material produced by rolling had a large amount of Gr element adhesion points and wide and deep furrows, adhesive wear also had occurred; after heat treatment, the material produced significantly less adhesion, the furrows were relatively shallow and narrow with some pitting and flaking, reflecting the obvious fatigue wear and abrasive wear characteristics. The wear surface of the 18Ni300 cladding layer manufactured by laser cladding before heat treatment showed obvious untidy edge furrows and adhesion, and there were abrasive chips adhering to the material surface, and adhesive wear occurred; after heat treatment, the material surface flatness was the best, and short furrows, abrasive chips, and craters appeared. The wear mechanism showed slight abrasive grain wear.

Acknowledgements

This work was supported by Key Research and Development Program of Liaoning Province (2022JH1/10800022). The authors declare no conflict of interest.

Data availability statement

The data presented in this study are available upon request from the corresponding author.

Conflict of interest statement

The authors declare no conflict of interest.

References

[1] Lu BH. Additive manufacturing—current situation and future. *Chin J Mech Eng*. 2020;31(01): 19–23. doi: 10.3969/j.issn.1004-132X.2020.01.003

[2] Tan CL, Zhou K, Ma W, Zeng DC. Research progress of laser additive manufacturing of maraging steels. *Acta Metall Sin-Engl*. 2019;56(01): 36–52. doi: 10.11900/0412.1961.2019.00129

[3] Global Maraging Steel Market Report By Product Type (Grade 200, Grade 250, Grade 300, Grade 350), By Application Coverage (Automotive & Racing Car, Aviation & Space, Defense, Medical Device, Sports, Others) And By Regions – Industry Trends, Size, Share, Growth, Estimation and Forecast, 2022–2030, https://www.valuemarketresearch.com/report/maraging-steel-market (Reference date: 20 December 2024).

[4] Kannan F, Leonard DN, Nandwana P. Optimization of direct aging temperature of Ti free grade 300 maraging steel manufactured using laser powder bed fusion (LPBF). *Mater Sci Eng: A*, 2021;817:141266. doi: 10.1016/j.msea.2021.141266

[5] Niu Y, Zhao P, Ning L, et al. Research status and application of ultra-high strength steel at home and abroad. *J Ordn Equip Eng*. 2021;42(7): 274–279. doi: 10.11809/bqzbgcxb2021.07.047

[6] Jiang ZH, Sun J, Berto F, Wang XI, Oian G. Fatigue and fracture behavior of AlSi10Mg manufactured by selective laser melting: a review. *Phys Mesomech*. 2023;26(4): 367–390. doi: 10.1134/S1029959923040001X

[7] Andrew W, Benoit MJ. A review of existing solidification crack tests and analysis of their transferability to additive manufacturing. *J Mater Process Technol*. 2023;320: 118090. doi: 10.1016/j.jmatprotec.2023.118090

[8] Guiru M, Jingdong Z, Jiachen L, Jiang Z, Gong Y, Zhao J. Impact of pore defects on laser additive manufacturing of Inconel 718 alloy based on a novel finite element model: thermal and stress evaluation. *Opt Laser Technol*. 2023;167: 109782. doi: 10.1016/j.optlastec.2023.109782

[9] Yizhen Z, Hang Z, Jianglong C, Sun X, Wang L, Xu X. An efficient pores suppression process design method for high strength BCC high entropy alloys via powder bed fusion. *J Manuf Process*. 2023:101: 371–385. doi: 10.1016/j.jmapro.2023.05.097

[10] Yan J, Zhou Y, Gu R, Zhang X, Quach W-M, Yan M. A comprehensive study of steel powders (316L, H13, P20 and 18Ni300) for their selective laser melting additive manufacturing. *Metals*. 2019;9(1): 86. doi: 10.3390/met9010086

[11] Di W, Deng G-W, Yang Y-Q, Chen J, Wu W-H, Wang H-L, Tan C-L. Interface microstructure and mechanical properties of selective laser melted multilayer functionally graded materials. *J Cent South Univ*. 2021;28(4): 1155–1169. doi: 10.1007/s11771-021-4687-9

[12] Mingcai P, Junqiang X, Ningning L, Yong P Zhou Q, Wang K. Microstructure and mechanical properties of the laminated heterostructured material with 316L stainless steel/18Ni300 maraging steel fabricated by WAAM. *Mater Sci Eng A*. 2023;881: 145300. doi: 10.1016/j.msea.2023.145300

[13] Zhenjiang Z, Chaofang D, Decheng K, Wang L, Xiaoqing N, Zhang L, Wu W, Zhu L, Li X. Influence of pore defects on the mechanical property and corrosion behavior of SLM 18Ni300 maraging steel. *Mater Charact*. 2021;182: 111514. doi: 10.1016/j.matchar.2021.111514

[14] Qun W, Jiaqi H, Li G, Yi Z, Peng J, Xinjua Y, et al. Electrochemical corrosion behavior of 18Ni300 maraging steel obtained by laser cladding deposition and selective laser melting in corrosive mediums: s comparative study. *J Mater Eng Perform*. 2022;31(10): 129425. doi: 10.1007/s11665-022-06849-7

[15] Zhongfa M, Xiangdong L, Hongru Y, Xiaodong N, Lujie Z, Xuefen X. Processing optimization, microstructure, mechanical properties and nanoprecipitation behavior of 18Ni300 maraging steel in selective laser melting. *Mater Sci Eng A*. 2022;830: 142334. doi: 10.1016/j.msea.2021.142334

[16] Weimin L, Zeyu Y, Qi G, Shufen L. Effect of energy density on the quality and properties of laser cladding 18Ni300. *J Laser Appl*. 2024;36(2): 022004. doi: 10.2351/7.0001240

[17] Zeyu Y, Weimin L, Shufen L, Qi G. Study on overlap rate and machinability of selected laser melting of maraging steel. *Mater Sci-Pol.* 2023;41(2): 368–382. doi: 10.2478/msp-2023-0028

[18] Ji X. Study on strengthening and toughening Mmechanism and property optimization of 18NI(350) ultra-high strength maraging steel. Yanshan University, 2021. doi: 10.27440/d.cnki.gysdu.2021.000411

[19] Lian G, Cao Q, Zheng Y, et al. Multichannel lap forming and powder utilization ratio of laser cladding. *J Mater Heat Treat*. 2023;44(2): 127–139. doi: 10.13289/j.issn.1009-6264.2022-0356

[20] Xinlei Luo, Meihong Liu, Zhenhua Li, et al. Influence of different heat source models on the calculated results of temperature field of selected laser melting 18Ni300. *Chin J Lasers*. 2021;48(14): 52–62. doi: 10.3788/CJL202148.1402005

[21] Bin L, Zezhou K, Zhonghua L, Jianbin T, Peikang B, Baoqiang L, Y Nie. Performance consistency of AlSi10Mg alloy manufactured by simulating multi laser beam selective laser melting (SLM): microstructures and mechanical properties. *Materials* (Basel). 2018; 11(12). doi: 10.3390/ma11122354

[22] Yang G, Yi-Lun H, Li-Chang Y, Zhangting W, Zhiqing Y, Mao-Lin C, et al. Ultrafast growth of high-quality monolayer WSe2 on Au. *Adv Mater*. 2017;29(29). doi: 10.1002/adma.201700990

[23] Yuhang Y, Jinhua L, Fangping Y, Xiangyu L. Effect of laser remelting on the organization and properties of WC/Ni-based coatings generated in situ by laser cladding. *J Manuf Process*. 2023;102: 501–5212. doi: 10.1016/j.jmapro.2023.07.075

[24] Badkoobeh F, Mostaan H, Rafiei M, Bakhsheshi-Rad HR, Ramakrishna S, Chen X. Additive manufacturing of biodegradable magnesium-based materials: design strategies, properties, and biomedical applications. *J Magnes Alloy*. 2023;11(03): 801–839. doi: 10.1016/j.jma.2022.12.001

[25] Liang Y, Ding W, Liu G, Traub J, Gu Z. Interlaced stacked hollow Cu2O dendrite for stable lithium metal anode. *Solid State Ionics*. 2024;410: 116530. doi: 10.1016/j.ssi.2024.116530

[26] Tang W, Yang X, Tian C, Xu Y. Microstructural heterogeneity and bonding strength of planar interface formed in additive manufacturing of Al–Mg–Si alloy based on friction and extrusion. *Int J Minerals*. 2022;29(09): 1755–1769. doi: 10.1007/s12613-022-2506-4

[27] Guoxing Q, Qing D, Xiaoming L, Xiang-dong X, Dongping Z. Strengthening effect of multiscale second phases in reduced activation ferrite/martensitic steel. *Steel Res Int*. 2021;93(4). doi: 10.1002/srin.202100430

[28] Jiangkai L, Zhubin H, Wei D, Xianggang R, Enyu G, Ninggiang S. Tailoring the microstructure and mechanical properties of laser metal-deposited Hastelloy X superalloy sheets via post heat-treatment. *Mater Sci Eng A*. 2023;884: 145546. doi: 10.1016/j.msea.2023.145546

[29] Kürnsteiner P, Wilms MB, Weisheit A, Barriobero-Vila P, Jägle EA, Raabe D. Massive nanoprecipitation in an Fe-19Ni-xAl maraging steel triggered by the intrinsic heat treatment during laser metal deposition. *Acta Mater*. 2017;129: 52–60. doi: 10.1016/j.actamat.2017.02.069

[30] Chen J, Feng B, Wang W, Liang Y, Zhang W, Xinzhu L, et al. Cobalt nanoparticles supported on nitrogen-doped carbon nanotubes for the efficient oxygen reduction reaction in Mg-air battery. *J Alloys Compd*. 2024;983: 173878. doi: 10.1016/j.jallcom.2024.173878

[31] ASM International Handbook Committee. Properties and selection:irons, steels, and high-performance alloys. *ASM Handbook*. Materials Park, Ohio: Materials Information Company, America. 1991;1872–1873. doi: 10.31399/asm.hb.v01.9781627081610

[32] Popovich VA, Borisov EV, Popovich AA, Sufiiarov VS, Masaylo DV, Alzina L. Functionally graded inconel 718 processed by additive manufacturing: crystallographic texture, anisotropy of microstructure and mechanical properties. *Mater Design*. 2017;114: 441–449. doi: 10.1016/j.matdes.2016.10.075

[33] Ming C, Tao L, Bowen S, Gong X. Study on critical bonding rate and flatness of laser cladding on inclined matrix. *Appl Laser*. 2023;43: 26–32. doi: 10.11896/cldb.23010049

[34] Li J, Wang X, Qi W, Tian J, . Laser nanocomposites-reinforcing/manufacturing of SLM 18Ni300 alloy under aging treatment. Materials Characterization, 2019;153. https://link.cnki.net/urlid/43.1239.TG.20230808.1558.002

[35] Guo W, Xing Z, Li P, et al. Research status of cold sprayed Cu-based composite coatings and post-process treatments . *Mater Rep*. 2024;38(19): 23010049. doi: 10.16490/j.cnki.issn.1001-3660.2021.07.021

[36] Zhang P, Yuan X-B, Zeng Z, et al. Influence of Fe content on microstructure and performance of powder metallurgy CuFe alloys. *Trans Nonferrous Metals Soc Chin.* 2023;1–24. https://link.cnki.net/urlid/43.1239.TG.20230808.1558.002

[37] Zhang T, Cheng B, Li W-Sh, et al. Tribological performance of low pressure cold spray Ni-based cermet composite coatings. *Surf Technol*. 2021;50(07): 203–211. doi: 10.16490/j.cnki.issn.1001-3660.2021.07.021

[38] Archard JF. Contact and rubbing of flat surfaces. *J Appl Phys*. 1953;24(8): 981–988 doi: 10.1063/1.1721448

[39] Zheng Y, Liu Y, Song Q, et al. High-temperature oxidation behavior and wear resistance of copper-based

composites with reinforcers of CZrSiO and Fe. *J Chin Soc Corros Protect*. 2020;40(02): 191–198. doi: 10.11902/1005.4537.2019.227

[40] Deng G, Tieu K, Lan X, Su L. Effects of normal load and velocity on the dry sliding tribological behaviour of CoCrFeNiMo 0.2 high entropy alloy. *Tribol Int*. 2020;144: 106116. doi: 10.1016/j.triboint.2019.106116

[41] An Q, Qi W, Zuo X. Microstructure and wear resistance of in-situ TiC reinforced Ti based coating by laser cladding on TA15 titanium alloy surface. *J Mater Eng*. 2022;50(04): 139–146. doi: 10.11868/j.issn.1001-4381.2020.000996

Received 2024-04-14
Accepted 2024-05-16